SUBSURFACE EXPRESSION OF A TERTIARY SALT WELD, GULF OF MEXICO

Christopher A-L. Jackson[1*]
Yue Zhang[1]
Donald A. Herron[2]
Peter J.R. Fitch[1]

[1]*Basins Research Group (BRG), Department of Earth Science and Engineering,*
Imperial College London, UK

[2]*Consultant, Sugar Land, Texas, USA*

**Corresponding author email: c.jackson@imperial.ac.uk*

ABSTRACT

Salt welds form due to expulsion and thinning of salt. Despite welds being ubiquitous in salt-bearing sedimentary basins, where they may trap large volumes of hydrocarbons, we know relatively little of their thickness and composition. We here use 3D isotropic Kirchhoff prestack depth migrated (KPSDM) seismic, borehole, and biostratigraphic data from the Atwater Valley protraction area of the Gulf of Mexico to constrain the thickness and composition of a tertiary salt weld. Seismic data image an 'apparent weld' (*sensu* Wagner and Jackson, 2011) at the base of a Plio-Pleistocene minibasin that subsided into thick allochthonous salt. Well data indicate the weld is in fact 'incomplete', being c. 24 m thick, and containing an upper 5 m thick halite and a lower 15 m thick halite, separated by a 4 m thick mudstone. The age and origin of the intra-weld mudstone is unclear, although we speculate it is: (i) Late Jurassic, representing material transported upwards from the autochthonous level within a feeder, and subsequently trapped as allochthonous salt thinned and welded, or; (ii) Pliocene, representing a piece of carapace material transported upwards atop and reworked from the crest of a feeder that fed the overlying, now-welded sheet. We show that even relatively modern, high-quality 3D seismic reflection data may be unable to resolve salt weld thickness, with the presence of a relatively thin remnant salt lending support to models of welding based on viscous flow. Furthermore, the halite-dominated character of the weld supports the hypothesis that tectonic purification occurs during flow of salt from autochthonous to allochthonous levels.

INTRODUCTION

Salt welds are ubiquitous in salt-bearing sedimentary basins, forming due to the complete expulsion of salt from below or between minibasins (Jackson and Cramez, 1989). Salt welds are economically important because, depending on their thickness and composition, they may represent barriers to fluid flow, and thus seal and help trap hydrocarbon accumulations (Rowan, 2004). Furthermore, weld thickness and composition reveal much about salt rheology and patterns of internal deformation (Kupfer, 1968; Wagner and Jackson, 2011; Jackson et al., 2014). Despite their importance and ubiquity, we have a rather poor understanding of the thickness or composition of subsurface welds; in some basins, this reflects a lack of borehole penetrations or, in relatively densely drilled basins, such as the Gulf of Mexico, a lack of access to these data. Where these data are available, such as in the Santos Basin, offshore Brazil they indicate that even high-quality 3D seismic reflection data may be unable to resolve the thickness or composition of welds, and that, at the primary weld level at least, welds may lack true 'salt', being halite- and potash-poor, being instead dominated by carbonate, anhydrite, and sandstone (Jackson et al., 2014; see also fig. 17 in Wagner and Jackson, 2011). This lithological partitioning suggests preferential expulsion of halite and potash salt from the autochthonous layer into flanking diapirs during viscous flow and welding. This process, which is termed 'differential purification by movement' by Kupfer (1968), implies that successive periods of salt flow, for example as salt ascends from autochthonous to allochthonous levels, will lead to relative enrichment in the more mobile components (e.g. halite, potash salts) of the original salt layer. This observation supports analytical and numerical models based on viscous-thinning of the salt during welding (Wagner and Jackson, 2011), which conclude it is difficult to fully remove salt from a weld by viscous flow alone because of boundary drag along the salt contacts (see also Cohen and Hardy, 1996; Hudec and Jackson, 2007). More specifically, the models of Wagner and Jackson (2011) suggest that a weld may contain anywhere from <1 m to up to c. 50 m of remnant salt, although they recognize that model-based predictions of remnant evaporite thickness in salt welds has hitherto been difficult to test due to a lack of data from natural welds (see Wagner, 2010; Hoetz et al., 2011; Liro and Holdaway, 2011; Rowan et al., 2012).

We here use 3D seismic reflection, borehole and biostratigraphic data from Block 8 in the Atwater Valley protraction area of the Gulf of Mexico (Fig. 1) to characterisation the subsurface expression of a tertiary salt weld. 3D seismic data allow us to define the geophysical expression and regional geological context of the weld, whereas borehole data allow us to constrain weld thickness and composition. Biostratigraphic data provide a rare opportunity to establish the precise age of the weld and subjacent strata, and to place the development of the weld and overburden in the context of the regional salt-tectonic framework. More specifically, our data allow us to explicitly test the following two hypotheses: (i) that allochthonous salt should be relatively enriched in the more mobile lithologies typically encountered at autochthonous levels; and (ii) that only several tens of metres of remnant salt should remain in a seismically defined weld.

GEOLOGICAL SETTING

The Gulf of Mexico formed in response to Triassic-Early Cretaceous rifting (e.g., Pindell and Dewey, 1982; Kneller and Johnson, 2011; Hudec et al., 2013b). Extension and subsidence allowed establishment of a restricted marine seaway, within which the Louann salt (Middle Jurassic) was deposited (e.g., Hazzard et al., 1947; Humphris, 1978; Salvador, 1987; Kneller and Johnson, 2011; Hudec et al., 2013a). Since then, in the northern Gulf of Mexico, this salt layer has been flowed to form a complex array of salt diapirs and sheets, canopies and welds, largely in response to loading of the autochthonous and then allochthonous salt levels by Mesozoic to Cenozoic sediments that are now preserved in a series of predominantly clastic-filled minibasins (Fig. 1B) (e.g., Diegel et al., 1995; Peel et al., 1995; Rowan, 1995; Pilcher et al., 2011).

Our study area is located in Block 8 of the Atwater Valley protraction area, on the south-western flank of the Mississippi Fan, northern Gulf of Mexico (Fig. 1). Water depths range from 650 to 1150 m. Here, the salt-tectonic framework is dominated by: (i) Miocene and older rocks contained in primary minibasins that overlie autochthonous salt; (ii) a series of diapiric feeders that separate primary minibasins and that connect upward to and feed salt sheets forming part of a regionally extensive canopy extending southwards to the Sigsbee Escarpment; and (iii) Plio-Pleistocene rocks contained in secondary minibasins that subsided into allochthonous salt and that locally welded to underlying primary minibasins (Fig. 1B).

DATASET

Seismic Data

The seismic volume used in this study is a subset of a large regional 3D survey, composed of multiple narrow-azimuth 3D seismic data sets acquired in 1995-1998 and subsequently reprocessed as a single survey in 2008. This subset covers an area of approximately 550 km^2 in the southwestern Mississippi Canyon (MC) and northwestern Atwater Valley (AT) protraction areas in the east-central Gulf of Mexico (Fig. 1A). 3D isotropic Kirchhoff prestack depth migrated (KPSDM) data, with a sample rate of 10 m, record length of 15 km, and final bin size of 25m x 25 m, were used for interpretation. The data were processed to zero phase, and all seismic displays in this paper follow a polarity convention in which, for a zero-phase wavelet, a positive reflection coefficient is represented by a central trough (plotted white on a variable-density display).

Borehole Data

We use data from exploration borehole AT-8 #1, which was drilled in 1997 in the eastern part of the study area (Fig. 2). The borehole penetrated clastic overburden, before penetrating the studied weld and terminating in underlying clastic rocks. Conventional borehole measurements include differential caliper, bulk density, sonic, gamma ray and neutron porosity, which together allow us to interpret the lithology of the weld, in addition to the sub- and suprasalt strata. Biostratigraphic data are also available in this borehole, allowing us to constrain the age of strata above and below the weld, and thus the weld itself.

METHODOLOGY

Well-to-Seismic Tie and Seismic Interpretation

We identified and mapped three key seismic horizons; (i) base allochthonous salt; (ii) top allochthonous salt; and (iii) top suprasalt mudstone (see below), in addition to the seabed (Figs 3). By mapping base allochthonous salt we were able to identify structural lows at the base of the sheet, which may represent feeders (Fig. 3A) (see Jackson and Hudec, 2017). Mapping top (Fig. 2B) and base (Fig. 2A) salt allowed us to construct a salt isopach (Fig. 2C), from which we identified areas of thin or welded salt. An overburden isopach, generated from ours map of top salt and seabed, revealed the location of secondary minibasins and their relationship to the identified salt weld (Fig. 2D).

Well-log Interpretation

We establish the thickness and composition of the salt weld via petrophysical analysis of wireline log data (cf. Jackson et al., 2014). We use a combination of logs to broadly differentiate between: (i) relatively coarse-grained, likely sandstone-prone lithologies; (ii) relatively fine-grained, likely mudstone-dominated lithologies; and (iii) non-clastic lithologies (e.g. evaporites) (Fig. 5) (Rider and Kennedy, 2011). We show that halite is characterised by relatively low GR values (60 - 75 API), low DT values (101 – 125 μs/ft), and low RHOB values (1.99 – 2.11 g.cm^{-3}). Sandstone occurring above and below the salt is also characterised by low GR values (50 - 70 API), but has moderate DT values (110 – 130 μs/ft) and RHOB values (1.99 – 2.23 g.cm^{-3}). Mudstone is differentiated from sandstone based on its relatively high GR values (50 – 110 API), moderate to high DT values (116 – 130 μs/ft) and RHOB values (2.14 – 2.31 g.cm^{-3}). We use the caliper log to identify poor borehole conditions, which may signify intervals of strata deformed due to flow of salt (left-hand log track in Fig. 4A and B) (cf. Hilchie, 1968; Theys, 1999).

Biostratigraphic Analysis

We calibrate biostratigraphic data from AT-8 to the biostratigraphic chart of the Gulf of Mexico Offshore Region, which is provided by the Bureau of Ocean Energy Management, Regulation and Enforcement from the United States Department of Interior (https://www.data.boem.gov/Paleo/Files/biochart.pdf; webpage accessed 15th November 2017). This chart covers regional and local markers, foraminiferal, planktonic and benthic markers, in addition to regional and local calcareous nannoplanktonic markers, spanning the Jurassic to Quaternary.

SEISMIC ANALYSIS OF THE SALT-TECTONIC STRUCTURE

Here we provide a brief description of the salt-tectonic structure of the study area and the structural context of the weld, focusing on the three main structural units: (i) sub-salt minibasins; (ii) allochthonous salt; and (iii) supra-salt minibasins.

Sub-salt Minibasins

Due to migration noise and residual multiples generated by overlying allochthonous salt, sub-salt minibasins are not well imaged in our seismic data. Locally, however, where overlying salt is relatively thin, we observe relatively continuous, variable amplitude, sub-horizontal to gently dipping reflections (Fig. 3). These reflections are truncated below allochthonous salt (or its equivalent weld) across a base salt unconformity that is typically steepest near inferred feeders (Fig. 3; see also below). In the northeastern part of the study area, immediately north of AT-8 #1, gently south-dipping strata within a sub-salt minibasin are truncated northward below more steeply dipping strata in a secondary minibasin; we interpret that the contact between these two minibasins is a secondary weld (Fig. 3E) (*sensu* Jackson and Cramez, 1989). AT-8 #1 penetrates the upper 163 m of a sub-salt minibasin, with well-log data (Fig. 4) indicating it contains a broadly continuous, conformable succession of Late Miocene to Late Pliocene deep-water clastics (Fig. 3E).

Allochthonous Salt

Several allochthonous salt bodies are present within the study area. The tops and bases of these bodies are characterised by regionally mappable, high-amplitude peak (positive) and trough (negative) reflections, respectively. The salt is itself characterised by very chaotic, low-amplitude reflections (Figs 3 and 6). The main allochthonous salt body is up to 5500 m thick, broadly U-shaped within the area imaged by our seismic data, and encircles at least the southern end of the minibasin penetrated by AT-8 #1 (Fig. 2C). Base salt is very rugose, being defined by at least five sub-circular structural lows that are up to 8 km in diameter and with up to 2 km of relief (Figs 2A and 3); although subsalt seismic imaging is poor, based on (i) their geometric similarity to features observed elsewhere in the Gulf of Mexico (e.g. Pilcher et al., 2011); (ii) their development at the base of a large allochthonous salt body; and (iii) their development adjacent to clearly truncated sub-salt strata, we interpret these features as the tops of diapiric feeders that rose from autochthonous levels, between and thus defining the sub-salt minibasins, and which fed the overlying allochthonous salt canopy (Jackson and Hudec, 2017). Allochthonous salt appears to locally welded; we describe the geophysical and geological expression of this weld below.

Supra-salt Minibasins

At least six, at least partially connected supra-salt minibasins overlie the allochthonous salt (i.e. minibasins 1-5) or its equivalent weld (i.e. minibasin 6) (see labels in Fig. 2D). These minibasins are up to 12 km wide and 6.5 km thick, with borehole data indicating they contain Plio-Pleistocene deep-water clastics (Fig. 4).

BOREHOLE EXPRESSION OF THE WELD AND SUPERJACENT STRATA

A salt weld, which we will later show is ‘apparent’, (terminology after Wagner and Jackson, 2011; see also Jackson et al., 2014), is developed in the east-central part of the study area (Fig. 2E, 3B and E). The weld is defined by two closely spaced seismic reflections, the uppermost being a positive (white) event defining a downward increase in impedance; this seismic response is consistent with acoustically soft, clastic-dominated sedimentary rocks in the supra-salt minibasin overlying acoustically harder, evaporite-dominated rocks within the weld (Fig. 6; see also P-wave log in Fig. 4 and data in Fig. 5). Immediately adjacent to AT-8 #1, the weld dips *c*. 28° southward and is thus conformable with underlying and overlying, broadly south-dipping reflections (Figs 3E and 6B). Directly below the weld, a c. 180 m thick package of relatively discontinuous, locally chaotic reflections is present, which is underlain by more continuous reflections (Fig. 6). North of AT-8 #1, the weld dips northward and steepens to *c*. 30°, cross-cutting the discontinuous/chaotic reflections described above, and separating sub- and suprasalt strata, truncating the former at a relatively high-angle (*c*. 45°) (Fig. 6B).

AT-8 #1 penetrates the central part of minibasin 5 and its underlying weld (Figs 2E, 3B, 3E, and 6). Log data from this borehole thus allow us constrain the petrophysical expression, thickness and composition of the weld (Fig. 4). At the approximate depth of the weld, as defined by our seismic mapping and tied to well control using a regional anisotropy-depth function for correction of seismic depths to well depths, well log data indicate that two anomalously low density, high neutron, low gamma ray intervals are present, separated by a 4 m thick mudstone (4412–4436 m; Fig. 4B). These upper and lower, anomalously low-density intervals, which are 5 m and 15 m thick respectively, plot toward the top-left of a standard neutron–density crossplot (the purple and pink points in Fig. 5), thus are petrophysically and, we infer below, compositionally distinct from the over- and underlying, clastic-dominated sequences. We also observe significant increases in the resistivity log measurements in these intervals (4–16 ohm.m; Fig. 4B), in addition to a relative increase in the 'change in caliper' measurement, which implies a 'softer' lithology that caused enlargement of the borehole during drilling (between 4412–4416 and 4425–4436 m; Fig. 4B). Based on these wireline log-derived observations, in addition to the broader salt-tectonic framework, we interpret that the petrophysically distinct intervals encountered between 4412-4436 m are halite. An alternative interpretation is that these intervals represent gas-bearing clastic rocks; however, we dismiss this interpretation based on the absence of gas indicators at deeper or shallower levels within the borehole. It is important to note that no biostratigraphic data were recovered in this interval, thus the age of the intra-weld mudstone is unknown.

Our petrophysical analysis indicates that the *c*. 180 m thick package of discontinuous seismic reflections directly below the weld is mudstone-dominated, having similar petrophysical characteristics to shallow and deeper mudstones (i.e. relatively high gamma-ray, high density and moderate porosity; Figs 4 and 5).

DISCUSSION

The geophysical and geological expression of salt welds

We have shown that good quality seismic reflection data can constrain the gross position of a subhorizontal tertiary salt weld. Seismic data cannot, however, determine the completeness or composition of the weld studied here, with borehole data indicating a few tens of metres of halite-dominated stratigraphy remain (cf. Jackson et al., 2014). Recognizing a complete weld or the composition of an incomplete weld may, therefore, be extremely challenging in the absence of borehole data, and incomplete welds might be erroneously interpreted as being complete, when in reality, a thin veneer of impermeable rock remains between adjacent country rocks. The results of our study support the recommendation of Jackson et al. (2014), who suggested that, until borehole data unequivocally demonstrate the absence of evaporite between flanking strata, the term 'apparent weld' be used to describe seismically defined welds.

Our observation that a c. 20 m thick sequences remains in the Atwater Valley salt weld is consistent with the predictions of analytical and numerical models presented by Wagner and Jackson (2011), which suggest natural salt welds formed by viscous flow alone may contain anywhere from $\ll$1 m to up to c. 50 m of remnant salt. Our data, and that from the Campos (Wagner and Jackson, 2011) and

Santos basins (Jackson et al., 2014), thus support the hypothesis of Wagner and Jackson (2011) that viscous flow is a good analytical approximation of the physical processes occurring during salt thinning and welding, but that viscous flow alone is unlikely to result in complete evacuation of a salt layer. However, it is important to note that a borehole, irrespective of the quantity and quality of data it provides, is only have a 1D sample point; it is possible that, away from this sample point, the weld may be complete.

Composition of salt welds

Our borehole data indicate the incomplete tertiary weld penetrated by AT-8 #1 is dominated by halite, and that other evaporite (e.g. anhydrite, potash salts) and non-evaporite lithologies, such as carbonate, are absent (Fig. 4). The composition of the weld differs strongly to that encountered in primary welds in the other salt-bearing sediment basins. For example, the Parati Weld, Santos Basin, offshore SE Brazil, which is 22 m thick, is halite-poor, being dominated by carbonate (40%) and anhydrite (40%), with minor amounts of sandstone (16%) and marl (4%). Similarly, halite-poor sequences are observed in incomplete primary welds penetrated by boreholes in the Campos Basin, offshore Brazil (see fig. 17 in Wagner and Jackson, 2011). In that location, 75 boreholes have penetrated multi-layered evaporites in the Retiro Member of the Lagoa Feia Formation (Aptian) (or its nonmarine equivalent). Forty-one of these boreholes penetrate evaporite-bearing sequences that are <100 m thick; of these, only 10 boreholes contain halite and anhydrite, with the remaining 31 boreholes containing only anhydrite.

The compositional variability encountered in primary and tertiary salt welds may reflect several factors, such as compositional variations in the autochthonous salt or preferential dissolution of mobile halite and bittern salts. For example, autochthonous salt comprising solely halite will only yield halite welds. An alternative interpretation is that compositional variability reflects a compositional and, more specifically, rheological control on the rate and ultimately magnitude of expulsion of different lithologies during salt thinning. For example, low viscosity lithologies, such as halite and potash salt, occurring in thick autochthonous salt in relatively large quantities, may be preferentially expelled from thinning salt before relatively high viscosity lithologies, such as carbonate, anhydrite and sandstone. As such, during welding, salt becomes relatively enriched in these less mobile, non-halite lithologies, which, due to the effects of boundary drag along the upper and low salt contacts, becomes trapped in the weld as the salt thinned (compare ‘differential purification by movement’; Kupfer, 1968; see also Wagner and Jackson, 2011 and Jackson et al., 2014). Salt structures flanking welds should thus be relatively enriched in mobile halite and potash salts, an observation that can be made indirectly inferred from seismic facies analysis (Van Gent et al., 2011; Fiduk and Rowan, 2012; Strozyk et al., 2012) or directly proven by borehole data (Jackson et al., 2014; 2015).

The differential purification by movement model suggests increasing compositional fractionation of salt should occur as the salt tectonic system evolves, with more viscous and/or denser units being stranded within the autochthonous level, trapped in primary welds, or stranded near the basal root of diapirs, and less viscous and/or less dense units forming the cores of these diapirs and, potentially, genetically related, allochthonous sheets and canopies. As such, supra-sheet/canopy minibasins should subside into 'purer' salt, comprised largely of halite and potash salts and, accordingly, underlying tertiary welds should be relatively rich in these rock types. Our data support this model, with a halite-rich weld being observed at relatively shallow levels in this salt-tectonic system. However, due to a lack of deep borehole data and post-depositional salt flow, we do not know the composition of autochthonous salt in the Gulf of Mexico, thus we cannot prove the halite-rich nature of the weld described here simply reflects strain-induced compositional fractional.

Although halite-dominated, the tertiary weld we describe here does contain a 4 m thick mudstone, which, despite being thin, accounts for 17% of the total weld 'fill'. The origin of this intra-weld mudstone is enigmatic; it may be the same age as the salt (i.e. Jurassic) and have ascended from autochthonous levels (if it is positively buoyant or, at least, not significantly denser than the salt), or be younger (i.e. post-Jurassic) carapace material (thin roof) from the initial feeder, which was then reworked from the crest of the sheet as it advanced, being trapped in spreading and then welding salt.

Implications for petroleum systems development in salt basins

This observation, along with the fact that various lithologies may remain in an incomplete weld, may directly impact hydrocarbon prospectivity in salt-tectonic basins. For example, the sealing capacity of an incomplete weld containing very low-permeability halite is likely to be higher than an incomplete weld containing permeable layers of carbonates and clastics. We may therefore speculate that primary welds, which may contains relatively little low-permeability halite and thus higher proportions of more permeable non-evaporitic lithologies, may be poorer seals and thus more susceptible to leakage. Additional data from primary, secondary, and tertiary welds, in addition to information on the hydrocarbon presence (or absence) in sub-salt strata, is required to test this hypothesis.

CONCLUSIONS

3D isotropic Kirchhoff prestack depth migrated (KPSDM) seismic data image the salt-tectonic structure and reveal the geophysical expression of a tertiary salt weld in the Atwater Valley protraction area of the Gulf of Mexico. This weld formed at the base of a Plio-Pleistocene minibasin that subsided into a thick allochthonous salt canopy fed by several diapiric feeders. Seismic reflection data suggest the weld is devoid of salt and is thus 'complete', although borehole data demonstrate the weld is in fact 'incomplete', being *c*. 24 m thick and containing an upper 5 m thick halite and a lower 15 m thick halite, separated by a 4 m thick mudstone of unknown age. The origin of the intra-weld mudstone is unclear, although it may be Late Jurassic, representing material transported upwards from the autochthonous level within a feeder, or Pliocene, representing carapace material incorporated into the canopy prior to thinning and welding. We show that even relatively modern 3D seismic reflection data may not resolve salt weld thickness, with the presence of a relatively thin layer of evaporites supporting analytically derived models of welding based on viscous flow. Furthermore, the halite-dominated character of the weld supports the hypothesis that tectonic purification occurs during flow of salt from autochthonous to allochthonous levels. In terms of hydrocarbon exploration, understanding the thickness and composition of material left in salt welds is important, with data presented here and in other studies suggesting that, for the same given thickness, the seal potential of tertiary welds may be higher than that of primary (or secondary) welds due to them being relatively enriched in low-permeability halite.

ACKNOWLEDGEMENTS

We thank Petroleum Geo-Services (PGS) for permission to use and show their proprietary seismic data, and Schlumberger for providing Petrel software to Imperial College via an Academic License Agreement. Biostratigraphic data for the AT-8 #1 were provided by Lexco Data Systems, L. P. in conjunction with Petroleum Geo-Services (PGS). We thank Mike Hudec, Yikuo Liu, and Connor O'Sullivan for very helpful discussions during the course of this study.

REFERENCES

Cohen, H.A., Hardy, S., 1996. Numerical modelling of stratal architectures resulting from differential loading of a mobile substrate, in G.I. Alsop, D.J. Blundell, and I. Davison, eds., Salt tectonics: Geological Society London Special Publications, 100, 265–273.

Diegel, F. A., J. F. Karlo, D. C. Schuster, R. C. Shoup, and P.R. Tauvers, 1995, Cenozoic structural evolution and tectono-stratigraphic framework of the northern Gulf Coast continental margin, in M. P. A. Jackson, D. G. Roberts, and S. Snelson, eds., Salt tectonics: A global perspective: AAPG Memoir 65, 109–151.

Fiduk, J.C., and M.G. Rowan, 2012, Analysis of folding and deformation within layered evaporites in Blocks BM-S-8 & -9, Santos Basin, Brazil, in G.I. Alsop, S.G. Archer, A.J. Hartley, N.T. Grant, and R. Hodgkinson, eds., Salt tectonics, sediments and prospectivity: Geological Society of London Special Publications, 363, 471-487.

Hazzard, R. T., W. C. Spooner, and B. W. Blanpied, 1947, Notes on the stratigraphy of the formations which underlie the Smackover Limestone in south Arkansas, northeast Texas, and north Louisiana: Shreveport Geological Society, Reference Report on Certain Oil and Gas Fields of North Louisiana, South Arkansas, Mississippi and Alabama, vol. II, 483–503.

Herron, D.A., 2011. First steps in seismic interpretation. Society of Exploration Geophysicists.

Hilchie, D.W. (1968). Caliper Logging – theory and practice. The Log Analyst, 9 (1), p. 3-12.

Hoetz, G., J. Steenbrinkl, N. Bekkers, A. Vogelaar, and S. Luthi, 2011, Salt-induced stress anomalies: an explanation for variations in seismic velocity and reservoir quality: Petroleum Geoscience, 17, 385-396.

Hudec, M.R., and M.P.A. Jackson, 2007, Terra infirm: understanding salt tectonics: Earth-Science Reviews, 82, 1-28.

Hudec, M. R., M. P. A. Jackson, and F. J. Peel, 2013a, Influence of deep Louann structure on the evolution of the northern Gulf of Mexico: AAPG Bulletin, 97, 1711–1735.

Hudec, M. R., I. O. Norton, M. P. A. Jackson, and F. J. Peel, 2013b, Jurassic evolution of the Gulf of Mexico salt basin: AAPG Bulletin, 97, 1683–1710.

Humphris, C. C., Jr., 1978, Salt movement on continental slope, northern Gulf of Mexico, in A. H. Bouma, G. T. Moore, and J. M. Coleman, eds., Framework, facies, and oil-trapping characteristics of the upper continental margin: AAPG, vol. 7, of, Studies in Geology, 69–86.

Jackson, C.A-L, Rodriguez, C.R., Rotevatn, A., and Bell R.E., 2014, Geological and geophysical expression of a primary salt weld: An example from the Santos Basin, Brazil, Interpretation, Vol: 2, Pages: SM77-SM89.

Jackson, C.A-L., Jackson, M.P.A., Hudec, M.R., and Rodriguez, C.R., 2015, Enigmatic structures within salt walls of the Santos Basin—Part 1: Geometry and kinematics from 3D seismic reflection and well data. Journal of Structural Geology, 75, 135-162.

Jackson, M.P.A., and C. Cramez, 1989, Seismic recognition of salt welds in salt tectonic regimes: Proceedings of the GCSSEPM Foundation 10th Annual Bob F. Perkins Research Conference, 66-71.

Jackson, M.P. and Hudec, M.R., 2017. Salt Tectonics: Principles and Practice. Cambridge University Press.

Kneller, E. A., and C.A. Johnson, 2011, Plate kinematics of the Gulf of Mexico based on integrated observations from the Central and South Atlantic: Gulf Coast Association of Geological Societies Transactions, 61, 283–300.

Kupfer, D.H., 1968, Relationship of internal and external structure of salt domes. In: J. Braunstein, and G.D. O'Brien, eds., Diapirism and diapirs: AAPG Memoir, 8, 79–89.

Liro, L., and S.M. Holdaway, 2011, Salt welds in the deepwater Gulf of Mexico – Uncertainties in the amount of remnant salt: seismic and well examples: AAPG Abstracts with Programs, 986760, p113.

Peel, F. J., C. J. Travis, and J. R. Hossack, 1995, Genetic structural provinces and salt tectonics of the Cenozoic offshore U.S. Gulf of Mexico: A preliminary analysis: AAPG Memoir, 65, 153–175.

Pilcher, R.S., Kilsdonk, B. and Trude, J., 2011. Primary basins and their boundaries in the deep-water northern Gulf of Mexico: Origin, trap types, and petroleum system implications. AAPG bulletin, 95(2), pp.219-240.

Pindell, J., and J.F. Dewey, 1982, Permo-Triassic reconstruction of western Pangea and the evolution of the Gulf of Mexico/Caribbean region: Tectonics, 1, 179–211.

Rider, M. and Kennedy, M. (2011). The Geological Interpretation of Well Logs (3rd ed.). Rider-French Consulting Ltd, Scotland.

Rowan, M. G., 1995, Structural styles and evolution of allochthonous salt, central Louisiana outer shelf and upper slope, in M. P. A. Jackson, D. G. Roberts, and S. Snelson, eds., Salt tectonics: A global perspective: AAPG Memoir 65, 199–228.

Rowan, M.G., 2004, Do salt welds seal? Proceedings of the GCSSEPM Foundation 24th Annual Bob F. Perkins Research Conference (Salt-Sediment Interactions and Hydrocarbon Prospectivity: Concepts, Applications, and Case Studies for the 21st Century), 390-403.

Rowan, M.G., Lawton, T.F., Giles, K.A., 2012, Anatomy of an exposed vertical salt weld and flanking strata La Popa Basin, Mexico. in G.I. Alsop, S.G. Archer, A.J. Hartley, N.T. Grant, and R. Hodgkinson, eds., Salt tectonics, sediments and prospectivity: Geological Society of London Special Publications, 363, 33-57.

Salvador, A., 1987, Late Triassic-Jurassic paleogeography and origin of Gulf of Mexico Basin: AAPG Bulletin, 71, 419–451.

Strozyk, F., H. Van Gent, J.L. Urai, and P.A. Kukla, 2012, 3D seismic study of complex intra-salt deformation: An example from the Upper Permian Zechstein 3 stringer, western Dutch offshore, in G.I. Alsop, S.G. Archer, A.J. Hartley, N.T. Grant, and R. Hodgkinson, eds., Salt tectonics, sediments and prospectivity: Geological Society of London Special Publications, 363, 489-501.

Theys, P. (1999). Log Data Acquisition and Quality Controls (2nd ed.). Editions Technip, Paris

Van Gent, H., J.L. Urai, and M. de Keijzer, 2011, The internal geometry of salt structures – a first look using 3D seismic data from the Zechstein of the Netherlands: Journal of Structural Geology, 33, 292-311.

Wagner III, B.H., 2010, An analysis of salt welding: Unpublished PhD dissertation, University of Texas at Austin, 218pp.

Wagner III, B.H., and M.P.A. Jackson, 2011, Viscous flow during salt welding: Tectonophysics, 510, 309-326.

FIGURE CAPTIONS

Fig. 1. (A) Simplified map showing the location of the study area. The location of the geoseismic profile shown in Fig. 1B is indicated. (B) Broadly NNW-trending geoseismic profile showing the approximate structural position and tectono-stratigraphic context of the study area. p=primary weld; t=tertiary weld. Note that no secondary welds are shown on this profile. TMM=top Middle Miocene; TPL=top Pliocene. The location of the profile is shown in Fig. 1A. Note that this line lies c. 50 km west of the study area (see Fig. 1A).

Fig. 2. (A) base salt depth map; (B) top salt depth map; (C) salt isopach; and (D) post-salt isopach. Locations of mapped seismic horizons shown in (A) and (B) are shown on Fig. 3.

Fig. 3. Broadly E-trending seismic profiles through the (A) north, (B) centre, and (C) south of the study area. (B) intersects through the studied salt weld and borehole AT-8 #1; (D) Broadly N-trending seismic profiles in the (D) west and (E) east of the study area. (D) and (E) intersects postulated salt feeders (Fig.

2E), with (E) also intersecting the studied salt weld and borehole AT-8 #1. s=secondary weld; t=tertiary weld. The locations of Fig. 6A and B are shown in (B) and (E), respectively.

Fig. 4. (A) Well-log and lithology data from the depth interval 4300-4500 m in AT-8 #1. The entire non-evaporitic sedimentary succession shown here is Upper Pliocene. Note the halite-rich character of the weld. For location of borehole, see Figs 2, 3B and D. (B) Details of the well-log expression of interval 4400-4500 in AT-8 #1. The weld and the main lithological subdivisions are indicated, with the colour-code referring to colours indicated in Fig. 5. The seismic polarity convention used for these seismic profiles and those in Fig. 6 are shown in (A).

Fig. 5. Neutron-density cross-plot of petrophysical data from the depth interval 4300-4500 m in AT-8 #1. Note the distinct expression of intra-weld halite, which is characterised by significantly lower neutron values than underlying or overlying clastics.

Fig. 6. (A) N-trending seismic profile (IL44638) through borehole AT-8 #1; (B) E-trending profile (XL6602) through borehole AT-8 #1. Both profiles illustrate the seismic character of the salt weld, and overlying and underlying stratigraphy. Note the distinctly chaotic seismic facies directly underlying the weld. The location of (A) is shown in Fig. 3B and the location of (B) in Fig. 3E.

Fig. 1

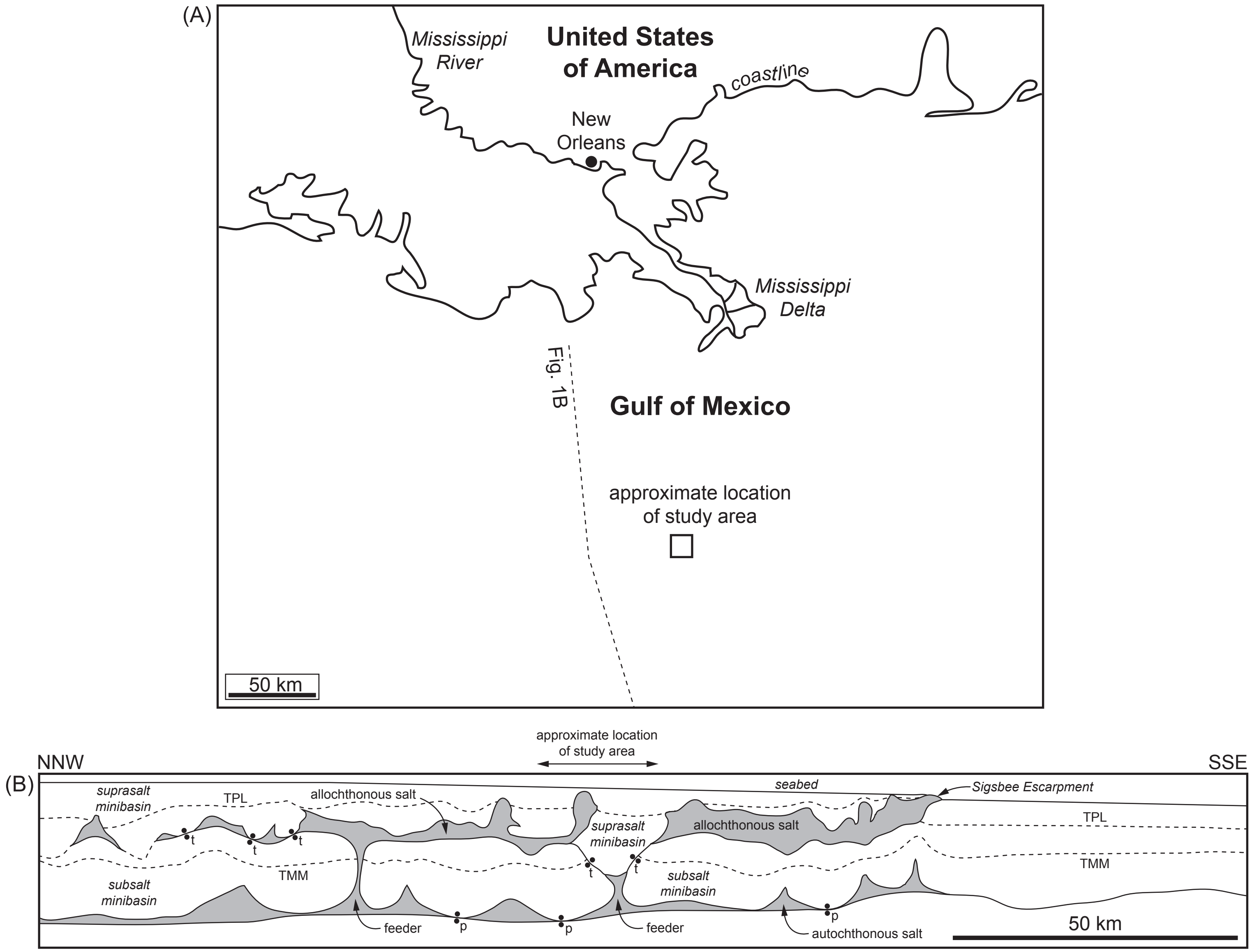
(A)
Mississippi River
United States of America
coastline
New Orleans
Mississippi Delta
Fig. 1B
Gulf of Mexico
approximate location of study area
50 km
(B)
approximate location of study area
NNW
SSE
seabed
Sigsbee Escarpment
suprasalt minibasin
TPL
allochthonous salt
suprasalt minibasin
allochthonous salt
TPL
t
t
t
t
t
TMM
TMM
subsalt minibasin
subsalt minibasin
feeder
p
p
feeder
autochthonous salt
p
50 km

Fig. 2

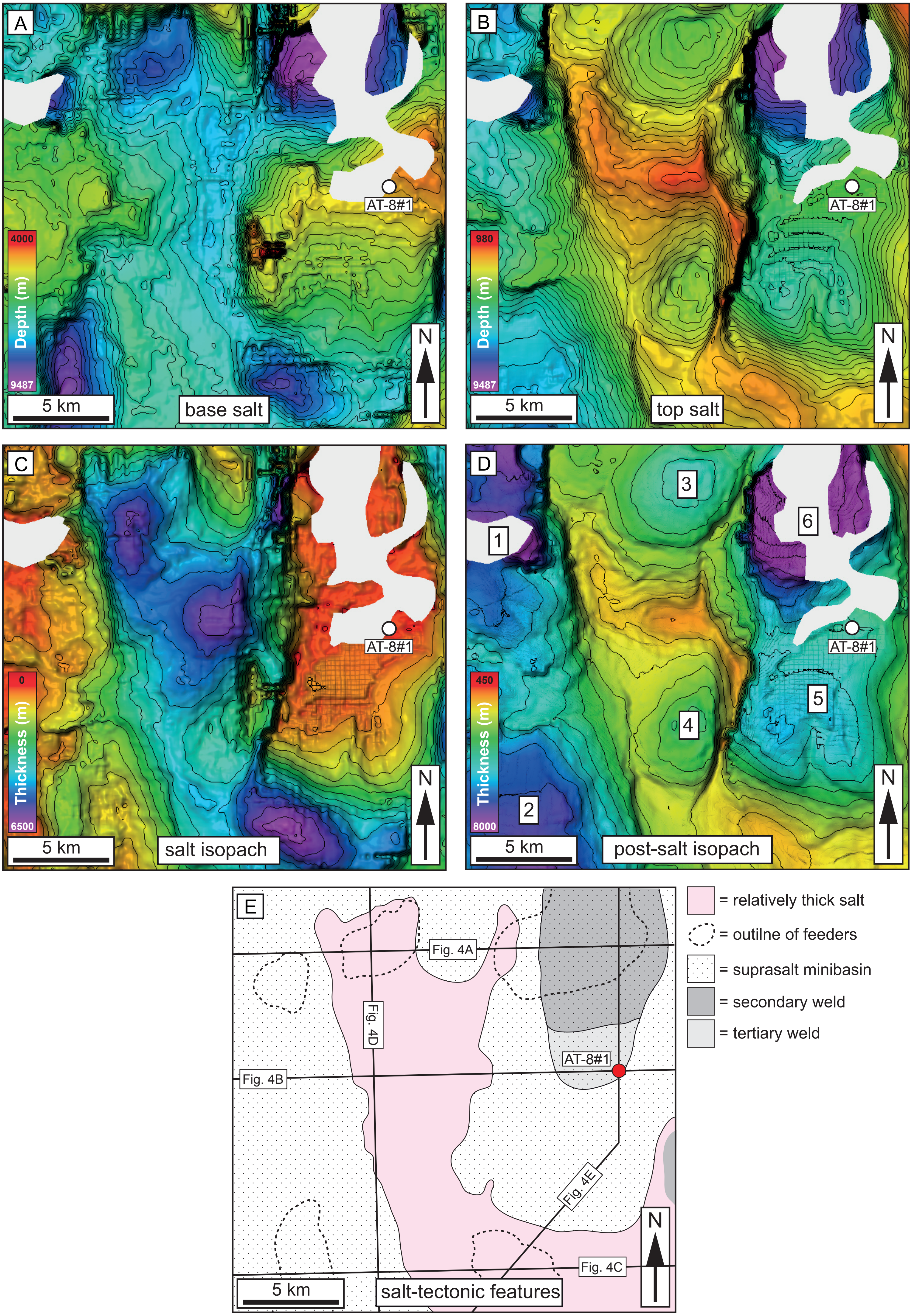
A
4000
Depth (m)
9487
AT-8#1
5 km
base salt
N
B
980
Depth (m)
9487
AT-8#1
5 km
top salt
N
C
0
Thickness (m)
6500
AT-8#1
5 km
salt isopach
N
D
1
2
3
4
5
6
450
Thickness (m)
8000
AT-8#1
5 km
post-salt isopach
N
E
Fig. 4A
Fig. 4D
Fig. 4B
Fig. 4E
Fig. 4C
AT-8#1
5 km
salt-tectonic features
N
= relatively thick salt
= outilne of feeders
= suprasalt minibasin
= secondary weld
= tertiary weld

Fig. 3

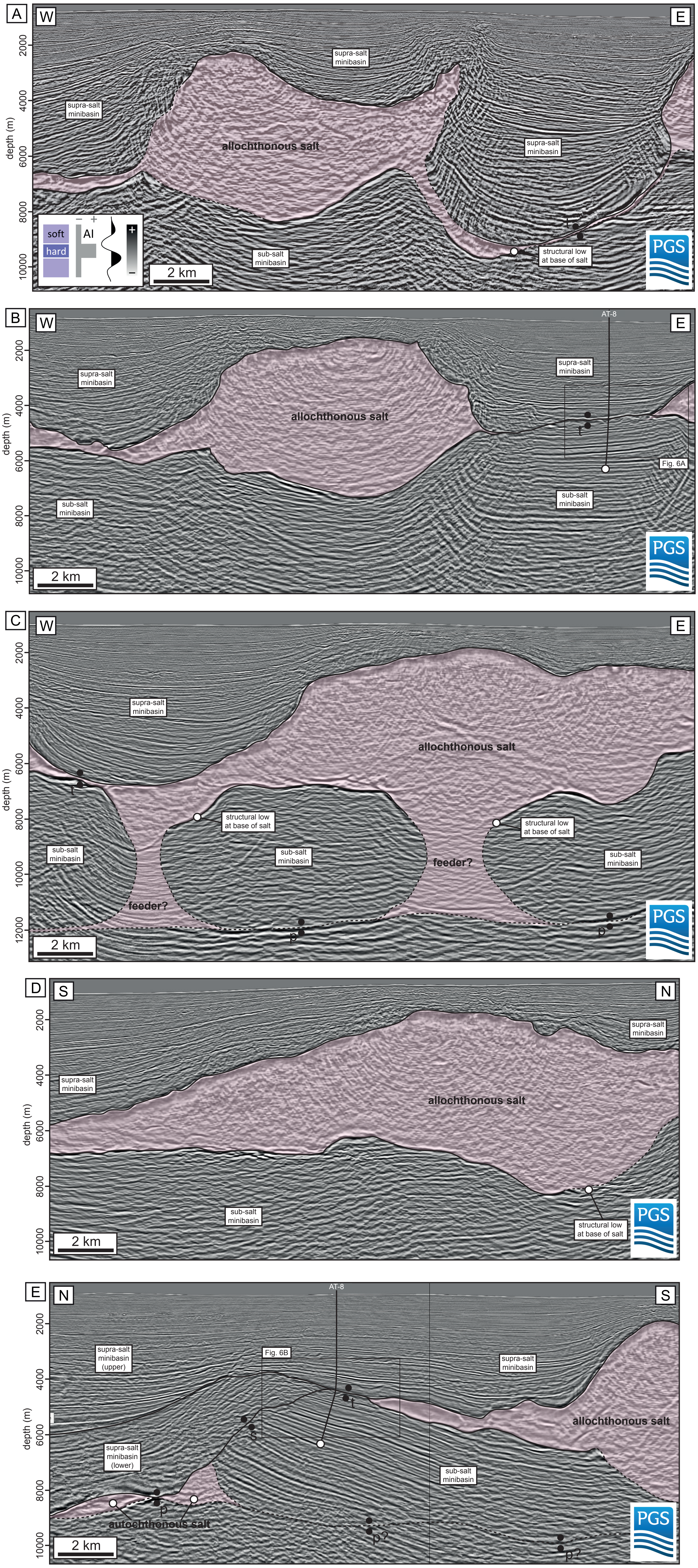
A
W
E
depth (m)
2000
4000
6000
8000
10000
supra-salt minibasin
supra-salt minibasin
supra-salt minibasin
allochthonous salt
sub-salt minibasin
structural low at base of salt
t
soft
hard
AI
−
+
2 km
PGS
B
W
E
AT-8
depth (m)
2000
4000
6000
8000
10000
supra-salt minibasin
supra-salt minibasin
allochthonous salt
t
Fig. 6A
sub-salt minibasin
sub-salt minibasin
2 km
PGS
C
W
E
depth (m)
2000
4000
6000
8000
10000
12000
supra-salt minibasin
allochthonous salt
t
structural low at base of salt
structural low at base of salt
sub-salt minibasin
sub-salt minibasin
sub-salt minibasin
feeder?
feeder?
p
p
2 km
PGS
D
S
N
depth (m)
2000
4000
6000
8000
10000
supra-salt minibasin
supra-salt minibasin
allochthonous salt
sub-salt minibasin
structural low at base of salt
2 km
PGS
E
N
S
AT-8
depth (m)
2000
4000
6000
8000
10000
supra-salt minibasin (upper)
Fig. 6B
supra-salt minibasin
t
s
allochthonous salt
supra-salt minibasin (lower)
sub-salt minibasin
p
autochthonous salt
p?
p?
2 km
PGS

Fig. 4

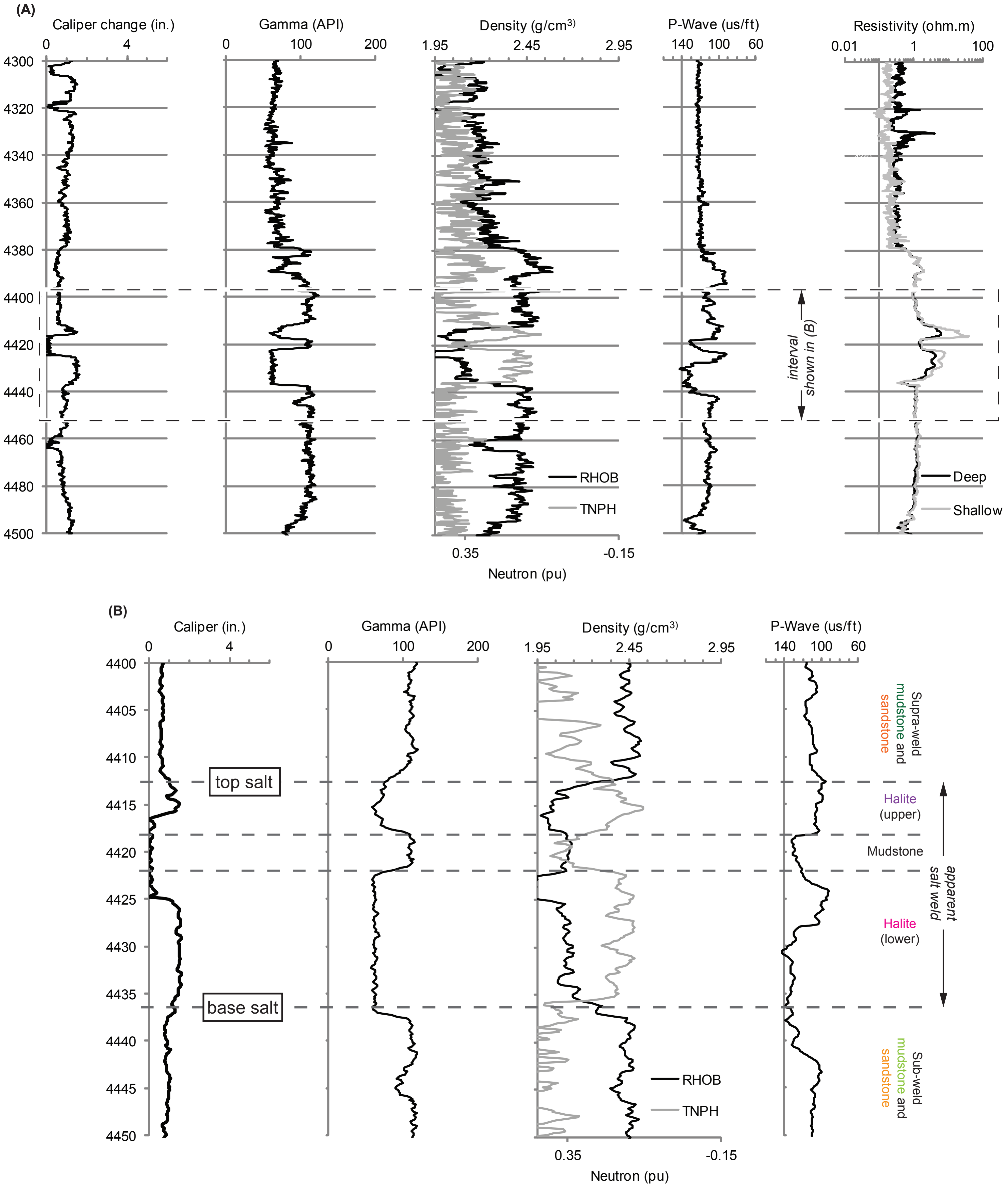
(A)
Caliper change (in.)
0
4
Gamma (API)
0
100
200
Density (g/cm3)
1.95
2.45
2.95
P-Wave (us/ft)
140
100
60
Resistivity (ohm.m)
0.01
1
100
4300
4320
4340
4360
4380
4400
4420
4440
4460
4480
4500
interval shown in (B)
RHOB
TNPH
Deep
Shallow
0.35
-0.15
Neutron (pu)
(B)
Caliper (in.)
0
4
Gamma (API)
0
100
200
Density (g/cm3)
1.95
2.45
2.95
P-Wave (us/ft)
140
100
60
4400
4405
4410
4415
4420
4425
4430
4435
4440
4445
4450
top salt
base salt
Supra-weld mudstone and sandstone
Halite (upper)
Mudstone
Halite (lower)
apparent salt weld
Sub-weld mudstone and sandstone
RHOB
TNPH
0.35
-0.15
Neutron (pu)

Fig. 5

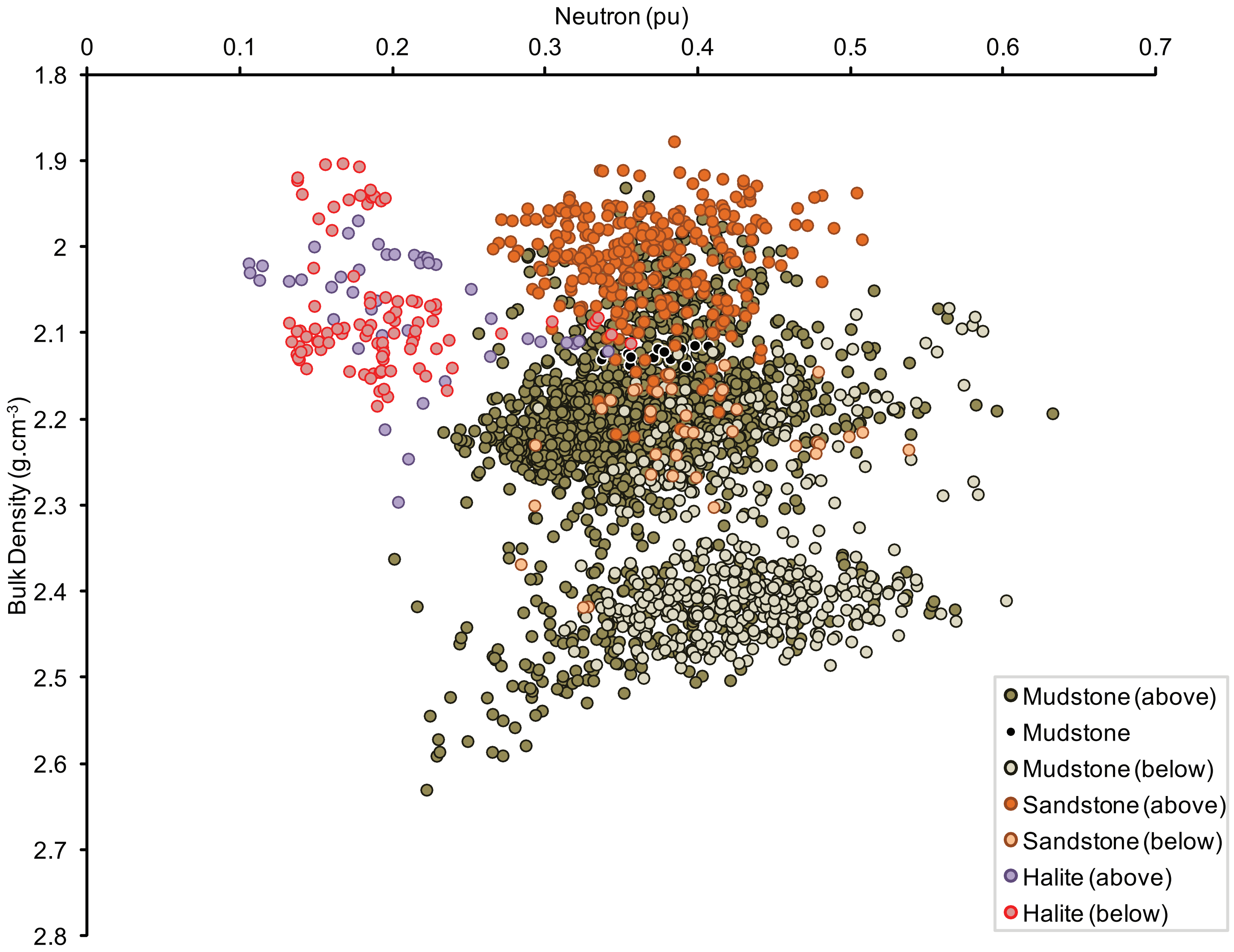
Neutron (pu)
0
0.1
0.2
0.3
0.4
0.5
0.6
0.7
Bulk Density (g.cm^{-3})
1.8
1.9
2
2.1
2.2
2.3
2.4
2.5
2.6
2.7
2.8
Mudstone (above)
Mudstone
Mudstone (below)
Sandstone (above)
Sandstone (below)
Halite (above)
Halite (below)

Fig. 6

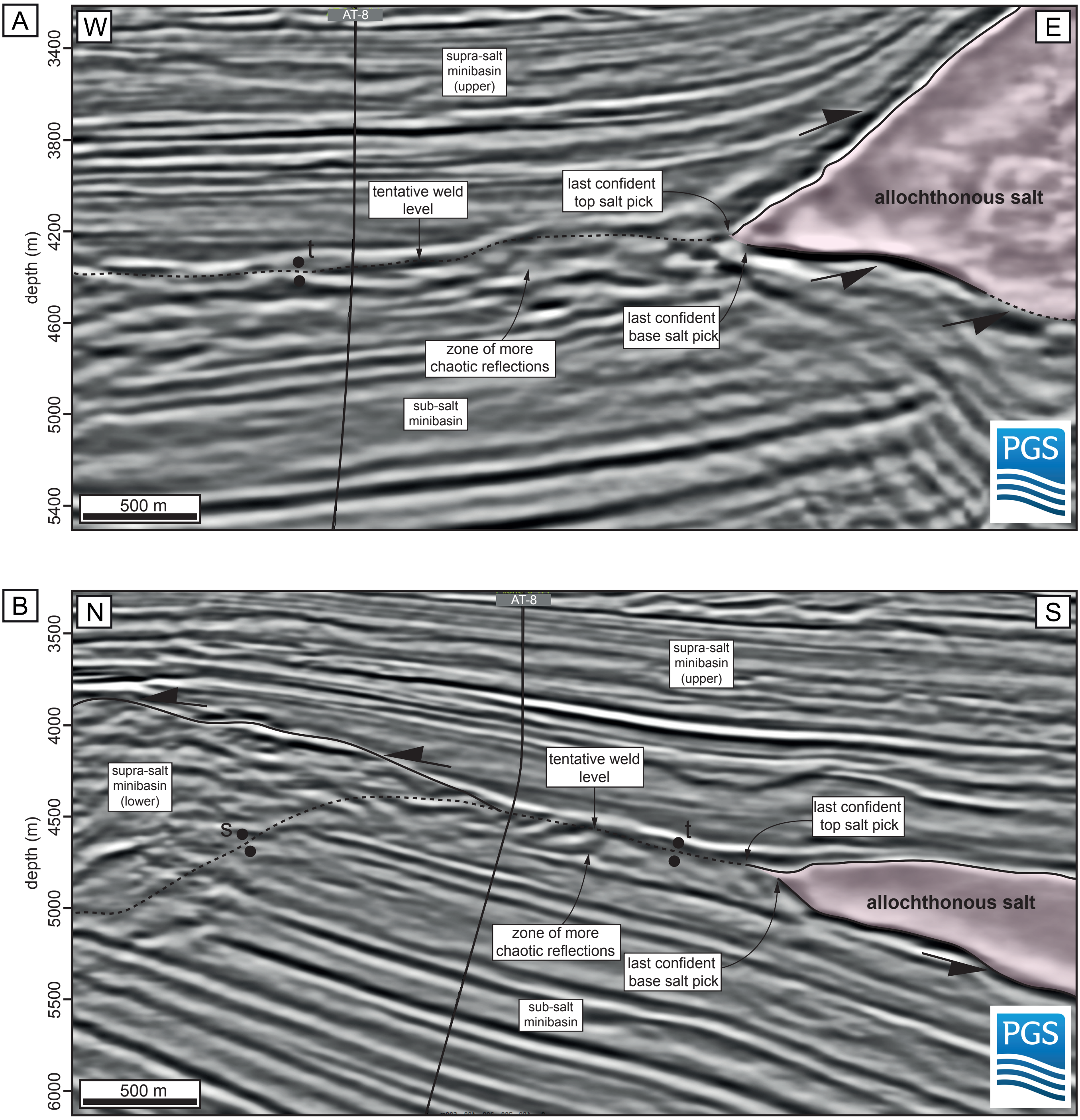
A
W
E
AT-8
supra-salt minibasin (upper)
tentative weld level
last confident top salt pick
allochthonous salt
t
last confident base salt pick
zone of more chaotic reflections
sub-salt minibasin
500 m
PGS
depth (m)
3400
3800
4200
4600
5000
5400
B
N
S
AT-8
supra-salt minibasin (upper)
supra-salt minibasin (lower)
tentative weld level
last confident top salt pick
s
t
allochthonous salt
zone of more chaotic reflections
last confident base salt pick
sub-salt minibasin
500 m
PGS
depth (m)
3500
4000
4500
5000
5500
6000